


Layered Materials **Very Important Paper**
How to cite: *Angew. Chem. Int. Ed.* **2021**, *60*, 8258–8267

International Edition: doi.org/10.1002/anie.202016334

German Edition: doi.org/10.1002/ange.202016334

Vacancy-Enabled O3 Phase Stabilization for Manganese-Rich Layered Sodium Cathodes

Biwei Xiao⁺, Yichao Wang⁺, Sha Tan⁺, Miao Song, Xiang Li, Yuxin Zhang, Feng Lin, Kee Sung Han, Fredrick Omenya, Khalil Amine, Xiao-Qing Yang, David Reed, Yanyan Hu, Gui-Liang Xu,* Enyuan Hu,* Xin Li,* and Xiaolin Li*

Abstract: Manganese-rich layered oxide materials hold great potential as low-cost and high-capacity cathodes for Na-ion batteries. However, they usually form a P2 phase and suffer from fast capacity fade. In this work, an O3 phase sodium cathode has been developed out of a Li and Mn-rich layered material by leveraging the creation of transition metal (TM) and oxygen vacancies and the electrochemical exchange of Na and Li. The Mn-rich layered cathode material remains primarily O3 phase during sodiation/desodiation and can have a full sodiation capacity of ca. 220 mAhg⁻¹. It delivers ca. 160 mAhg⁻¹ specific capacity between 2–3.8 V with > 86 % retention over 250 cycles. The TM and oxygen vacancies performed in the sodiated material enables a reversible migration of TMs from the TM layer to the tetrahedral sites in the Na layer upon de-sodiation and sodiation. The migration creates metastable states, leading to increased kinetic barrier that prohibits a complete O3-P3 phase transition.

Introduction

Na-ion batteries with gravimetric energy density potentially comparable to some Li-ion batteries and the sources widely available, have been pursued persistently for grid energy storage and low speed vehicles.^[1] Mn-rich (Mn > 50 %) layered oxide with high energy density and low-cost have been explored extensively in Li-ion batteries and even more in Na-ion battery cathode development.^[2] The large size

of Na-ions affects the stacking of layers and hence further complicates the structure of these layered Na-ion materials.^[1c,3] Layered Na-ion cathode materials are categorized into two families depending on the occupation site of the Na-ions, which include the trigonal prismatic (P-type) and octahedral (O-type) ones.^[4] Two of the most often studied cases are P2- and O3-type materials, in which “2” and “3” represent the number of edge-sharing transition metal oxides (TMO₆) octahedra layers in each repeating unit.^[5]

In general, O3-structured layered materials deliver higher capacity in a voltage range of 2–4 V, but the diffusion of Na-ions involves face-shared octahedral-tetrahedral-octahedral migration that can often lead to limited rate capability.^[6] P2-structured layered material, on the other hand, has relatively lower capacity within the same potential window, but the face-shared trigonal prismatic sites provide open pathway for the Na-ion diffusion.^[7] O- and P-type structures can be interchangeable upon de-sodiation and sodiation. In an O3-type cathode, the phase change of O3-P3 happens at relatively low potential with the layers gliding to minimize the Na-ion diffusion barrier. In a P2-type cathode, the phase change of P2-O2 happens at a relatively high potential when the amount of Na-ions in the layers is too low to shield the electrostatic repulsion force that results in the layer gliding.^[8] In both O3 and P2 materials, the phase transition involves tremendous volume change to the material, which, along with various Na orderings, greatly jeopardize the structural stability, causing

[*] Dr. B. Xiao,^[†] Dr. F. Omenya, Dr. D. Reed, Dr. X. L. Li

Energy & Environment Directorate
Pacific Northwest National Laboratory
Richland, WA 99352 (USA)
E-mail: xiaolin.li@pnnl.gov

Y. Wang,^[†] Prof. X. Li
John A. Paulson School of Engineering and Applied Sciences
Harvard University, Cambridge, MA 02138 (USA)
E-mail: lixin@seas.harvard.edu

S. Tan,^[†] Dr. X.-Q. Yang, Dr. E. Hu
Chemistry Division, Brookhaven National Laboratory
Upton, NY 11973 (USA)
E-mail: enhu@bnl.gov

Dr. M. Song
Physical and Computational Sciences Directorate
Pacific Northwest National Laboratory
Richland, WA 99352 (USA)

Dr. X. Li, Prof. Y. Hu
Department of Chemistry and Biochemistry
Florida State University, Tallahassee, FL 32306 (USA)



Y. Zhang, Prof. F. Lin
Department of Chemistry, Virginia Tech
Blacksburg, VA 24061 (USA)

Dr. K. S. Han
Environmental Molecular Sciences Laboratory
Pacific Northwest National Laboratory
Richland, WA 99352 (USA)

Dr. K. Amine, Dr. G. Xu
Chemical Sciences and Engineering Division
Argonne National Laboratory
9700 South Cass Avenue, Lemont, IL 60439 (USA)
E-mail: xug@anl.gov

Dr. K. Amine
Materials Science and Engineering, Stanford University
Stanford, CA 94305 (USA)

[†] These authors contributed equally to this work.

 Supporting information and the ORCID identification number(s) for the author(s) of this article can be found under:
 <https://doi.org/10.1002/anie.202016334>.

the performance decay in layered sodium cathode materials.^[9] With the above discussion in mind, it is essential to minimize the detrimental effects induced by phase transitions for high performance layered oxide cathodes.

Among the efforts to stabilize the structure and improve the material performance, introduction of dopants usually is the first to be explored.^[10] Significant progress has been made on improving the cycling stability,^[11] even though the electrochemically inactive dopants often reduce the capacity. Constructing a composite of P2 and O3 phases is also studied, as it was found that the volume change can be relieved by the interlocking of these two phases.^[12] It is worth noting, however, that the P2 phase requires Na-ion deficiency, which has to be considered if the full-cell efficiency is a concern.^[13]

As the root cause of phase transition is a lack of screening to the electrostatic repulsion forces of the lattice oxygen and the subsequent gliding of layers, a possible strategy to alleviate such a process would be to introduce a mechanism that can 1) reduce the repulsion force of lattice oxygen and/or 2) act as a shield when Na-ions are removed. To enable such a mechanism, one may reduce the net charge of the lattice oxygen (that is, create oxygen vacancies) or introduce a “reversible” TM migration to the alkali metal layer upon charging/discharging. The “reversible” migration here means TM moves between the alkaline layer and TM layer, while it does not necessarily mean back to the same site. One typical material that simultaneously garners these two effects is Li and Mn-rich layered cathode material (LRNMC). The removal of Li from the TM layer and the release of oxygen during the first de-lithiation process can lead to the creation of TM and oxygen vacancies.^[14] The TMs next to the TM vacancies, particularly Mn, have strong tendency to migrate to the tetrahedral vacancies in the adjacent Li layer.^[15] The reversibility of this migration can be essentially achieved by inhibiting further migration from the tetrahedral sites into the adjacent octahedral sites within the Li layer via limiting the voltage.

To verify the presumption, in this present study, LRNMC material after electrochemical de-lithiation was evaluated for the Na intercalation/de-intercalation correlations with TM and oxygen vacancies. A combination of systematic characterizations and computational simulations reveals that the pre-built vacancies enable TM migrations into the tetrahedral sites in the Na layer once de-sodiation starts and moving back to the TM layer at sodiation state. It results in a highly stable O3-type structured Na and Mn-rich layered cathode material with intermediate metastable states during de-sodiation/sodiation. The TM migration creates the kinetic barrier that inhibits a complete O3-P3 phase transition, hence leading to stabilized performance. Moreover, even with reduced inter-layer distance down to 5.0 Å, the diffusion of Na-ions in the layer is not negatively impacted, most probably owing to the presence of oxygen vacancies and metal oxide layer distortions. The material has a full sodiation capacity of $\approx 220 \text{ mAh g}^{-1}$. It can deliver $\approx 160 \text{ mAh g}^{-1}$ specific capacity between 2–3.8 V with $> 86\%$ retention over 250 cycles. This work reveals an approach of introducing vacancies to reach high cycling capacity without activating the oxygen redox and stabilize the structure from forming the P3 phase. The

understanding can be leveraged in the development of low-cost and high-performance cathode materials for various kinds of batteries.

Results and Discussion

Li and Mn-rich layered oxides of $\text{Li}_{1.2}[\text{Mn}_{0.66}\text{Co}_{0.17}\text{Ni}_{0.17}]_{0.8}\text{O}_2$ (LRNMC) was used as the model material. The ratio between Mn:Co:Ni of the pristine LRNMC measured by inductively coupled plasma atomic emission spectroscopy (ICP-AES) is 67:16:17, which confirms the designed composition. XRD pattern of the pristine LRNMC and its Rietveld refinement results (Supporting Information, Figure S1a and Table S1) and its cycling performance (Supporting Information, Figure S1b,c) are consistent with literature results.^[16] Figure 1a shows two sets of curves: 1) de-lithiation to 4.6 V followed by lithiation and 2) de-lithiation to 4.6 V followed by sodiation and de-sodiation (the two de-lithiation curves overlapped with each other). It is known that the de-lithiation curve with a cut-off voltage of 4.6 V (vs. Li/Li⁺) has two typical regions: 1) the region below 4.4 V relates to the removal of Li from the Li layers and 2) the following plateau above 4.4 V corresponds to the removal of Li from the TM layers (the de-lithiated LRNMC material is denoted as LRNMC4.6 throughout the paper).^[14a] Lithiation of this sample shows a solid solution behavior and a lithiation capacity of 250 mAh g^{-1} (blue curves). The red curves are the 1st sodiation/desodiation processes of the LRNMC4.6. First sodiation to 2 V (vs. Na/Na⁺) results in a remarkably high capacity of 220 mAh g^{-1} (the fully sodiated material is denoted as NaLRNMC4.6).

Based on the sodiation capacity, the composition of the sodiated material is estimated to be $\text{Na}_{1-x}\text{Li}_x[(\text{Mn}_{0.66}\text{Co}_{0.17}\text{Ni}_{0.17})_{0.8}\square_{0.2}]\text{O}_{2-y}$, where x is the amount of remaining Li in the structure, y is the oxygen released and \square represents the vacancies left after removing Li from the TM layers. The value of x is supposed to be very low considering the de-lithiation capacity has met the theoretical capacity (see detailed calculation in the Supporting Information, Figure S2). ICP-AES results have shown that the ratio of Na/TM in NaLRNMC4.6 is 1.18. Compared with the regular layered material with a NaTMO_2 stoichiometry and a Na/TM ratio of 1, this composition can be considered as “pseudo-Na-rich”. As it is not possible to intercalate more than 1 unit of Na into a NaTMO_2 , the Na/TM value above 1 is ascribed to the TM deficiency. ICP result can not differentiate the TM in TM layer or Na layer. If by any chance there is TM in the Na/Li layer, there has to be more TM vacancies in the TM layer since the total amount of TM is constant. In the case of layered Li cathode material, Dahn et al. have found that TM vacancies result in Li-rich composition with conventional layered structures, and it is able to promote high reversibility.^[17] In the case of layered Na cathode materials, the presence of vacancies in the TM layer was found to promote the oxygen activity at high voltage above 4.1 V (vs. Na/Na⁺).^[18] The involvement of oxygen activity increases the capacity at the expense of stability. It was intentionally

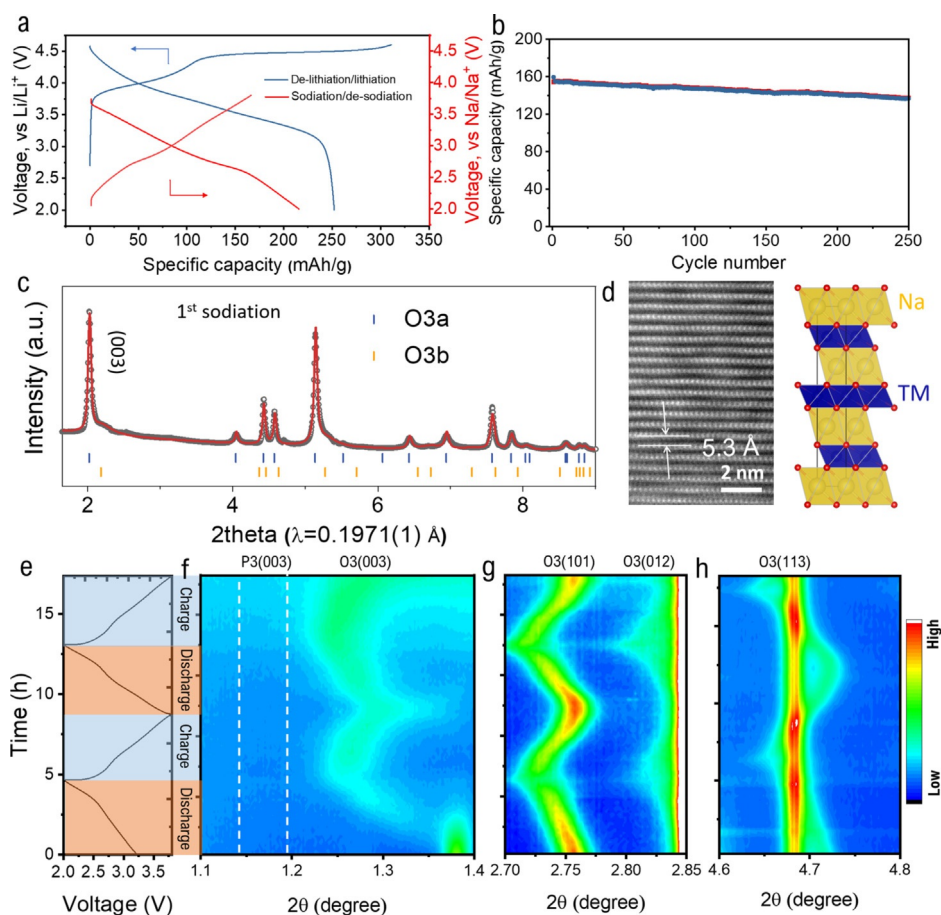


Figure 1. a) Curves of de-lithiation to 4.6 V (LRNMC4.6), lithiation to 2 V, sodiation of LRNMC4.6 to 2 V (NaLRNMC4.6) and its de-sodiation to 3.8 V. b) Cycling performance of NaLRNMC4.6 at 125 mA g⁻¹. c) ex situ synchrotron XRD of NaLRNMC4.6 after 1st sodiation ($\lambda = 0.1971(1)$ Å). d) HAADF image of the NaLRNMC4.6 after 1st sodiation. e)–h) in situ HEXRD measurement of the sodiation/de-sodiation of LRNMC4.6 ($\lambda = 0.117418(\pm 0.15\%)$ Å) at 12 mA g⁻¹ between 2–3.8 V (vs. Na/Na⁺).

avoided by restricting the voltage limit to 3.8 V (vs. Na/Na⁺) in this study that aims at revealing the effect of TM migration to the phase evolution. The charge/discharge curves of the 1st sodiation/desodiation in Figure 1a also show no obvious plateau or steps that are generally associated with phase transitions and/or charge/vacancy ordering. The cycling performance is shown in Figure 1b and the Supporting Information, Figure S3. Figure 1b is the stability test conducted under 125 mA g⁻¹ between 2–3.8 V after the 1st sodiation process. The material delivers an initial capacity of 160 mA h g⁻¹ and 86% capacity retention over 250 cycles. Such a high capacity within a narrow voltage window of 2–3.8 V and stable performance is hardly seen in Mn-rich layered Na cathode materials.^[3b,13,19]

Figure 1c shows the synchrotron X-ray diffraction (sXRD) pattern of NaLRNMC4.6 at the 1st sodiation state (2 V vs. Na/Na⁺) fitted by the Le Bail method.^[20] It shows two types of O3 phases, both of which belong to the *R3m* space group. Detailed fitting results are shown in Table S2. O3a has an interlayer spacing of ca. 5.4 Å, corresponding to the Na-bearing O3 phase. O3b has an interlayer spacing of 5.0 Å, which is associated with the unsodiated regions. Figure 1d shows the high-angle annular dark field scanning transmission

electron microscopy (HAADF-STEM) image of the O3a phase in NaLRNMC at the 1st full sodiation state. The interlayer lattice spacing measured is 5.3 Å, consistent with the value of an O3 structure.^[6] O3b phase HAADF-STEM image is not shown due to its low presence in the particles.

Mn-rich layered sodium cathode materials generally have a strong tendency to form P-type instead of O-type structures.^[13] To demonstrate the uniqueness of the O3 phase of NaLRNMC4.6, we have synthesized two other materials by mixing the transition metal hydroxide precursors with alkali metal sources with subsequent calcination. The composition was set to be Na_x(Mn_{0.66}Co_{0.17}Ni_{0.17})O₂ and Na_x[Li_{0.2}(Mn_{0.66}Co_{0.17}Ni_{0.17})_{0.8}]O₂, with *x* being 1 during synthesis. XRD patterns (Supporting Information, Figure S4a) show that the Na_x(Mn_{0.66}Co_{0.17}Ni_{0.17})O₂ material has a P2 structure, and the Na_x[Li_{0.2}(Mn_{0.66}Co_{0.17}Ni_{0.17})_{0.8}]O₂ is composed of P2 structure with a very tiny fraction of O3 structure.^[12b] Theoretical calculation has demonstrated that the phase stability of P2 phase will be broken when the stoichiometry of Na exceeds 0.9, therefore, the actual *x* values in the Na_x(Mn_{0.66}Co_{0.17}Ni_{0.17})O₂ and Na_x[Li_{0.2}(Mn_{0.66}Co_{0.17}Ni_{0.17})_{0.8}]O₂ samples should be lower than the set value during synthesis.^[13] P2-structured materials are known to have low capacity

within narrow voltage range, and the P2-structured $\text{Na}(\text{Mn}_{0.66}\text{Co}_{0.17}\text{Ni}_{0.17})\text{O}_2$ has only 60 mAh g^{-1} capacity between 2–3.8 V (Figure S4b,c). NaLRNMC4.6 at the 1st sodiation state, despite having the same Mn-rich TM stoichiometry with the directly synthesized P2 material, can be stabilized in O-type structure instead of P-type, which is supposed to be associated with the presence of vacancies.

The phase evolution detail of the sodiation/de-sodiation process was traced by synchrotron in situ high-energy XRD (HEXRD). Figures 1 e–h show the contour plot while the line plot is shown in the Supporting Information, Figure S5. Figure 1 e is the sodiation/de-sodiation voltage curve against testing time, where the starting point is the XRD of delithiated LRNMC vs. Na metal in sodium electrolyte. Figure 1 f reveals the evolution of the (003) peak. The O3 (003) peak of the LRNMC4.6 is at $\approx 1.38^\circ$ at the beginning of sodiation and it does not change much until the discharge voltage reaches 2.8 V (vs. Na metal), where a new peak at around 1.3° starts to emerge. It is assigned to the expanded (003) plane due to the intercalation of large-sized Na-ions. Upon full sodiation, the (003) plane expands to the maximum with the peak shifting to ca. 1.25° , corresponding to an interlayer spacing of 5.4 Å, corroborating the ex situ XRD results in Figure 1 c. The value is still outside of the P3 phase (003) plane range ($1.15\text{--}1.2^\circ$), confirming the fittings of O3 phases in Figure 1 c.^[21] The first sodiation was also accompanied with the negative shift of other diffraction peaks such as (101), (012), and (113) shown in Figure 1 g,h. They can be ascribed to the reduction of TMs and in-plane expansion.^[22]

A striking phase evolution is observed at de-sodiation, where 1) (003) plane shrinks and the peaks shifts to high angle; 2) no P3 (003) peak was observed. The (003) peak shifts to a higher angle throughout the de-sodiation process, demonstrating a contraction of the interlayer spacing. At the end of de-sodiation, the interlayer spacing was calculated to be only 5.0 Å. This is contradictory to conventional observations of O3-type cathode materials,^[11a] as well as the de-sodiation behavior of the Na-ion exchanged $\text{LiNi}_{1/3}\text{Co}_{1/3}\text{Mn}_{1/3}\text{O}_2$ (NMC333) cathode (Supporting Information, Figures S6, S7). Normally, Na-ions shield the electrostatic repulsion forces of the lattice oxygen, removing the Na-ions would lead to an interlayer expansion, while in some O3-type materials, only at the end of de-sodiation when the voltage is above 4.0 V, a monoclinic O1 phase with low interlayer spacing may emerge.^[9a,23] In this study, the interlayer expansion did not happen for NaLRNMC4.6, nor did the O3 to P3 phase transition when removing Na-ions out of the layered structure. Extensive selected area electron diffraction (SAED) and STEM-HAADF study have been carried out on the NaLRNMC samples charged to 3.0 V (a voltage that in situ XRD shows layer contraction) to check the possibility of any early formation of O1 phase. The typical results obtained at various locations and particles (Supporting Information, Figure S8) show representative O3a phase with the interlayer spacing of 5.3 Å and slight distortion. The absence of O1 phase implies that the migration of TMs to the tetrahedral sites is more likely to be the reason for the layer contraction during charge. The lack of obvious interlayer contraction in TEM is probably due to that the TMs are unstable at the

tetrahedral sites and return to the TM layer before the ex situ characterizations.^[19b]

It is also anomalous that the in situ sample displays broad (003) peaks compared with the ex situ HEXRD patterns (Figure 1 c) while other peaks remain narrow and intense (Supporting Information, Figure S5). No such peak dampening effect was observed in the control experiment with the in situ XRD of the sodiation/de-sodiation of Na ion exchanged NMC333 that was de-lithiated to 4.5 V (vs. Li/Li⁺) (Supporting Information, Figures S6, S7). The vacancies in the TM layers, which are the major difference between these two cases, play a pivotal role to the anomalous phenomena of phase transition and interlayer distance change. The pre-formed vacancies in LRNMC4.6 enable easy migration of TMs, similar to what we have observed in the iron-containing layered oxide cathodes at high Fe compositions.^[24] LRNMC4.6 with TM and O vacancies in the TM layer has significantly reduced the migration barrier of the adjacent TM. It is highly possible that these TMs migrated into the tetrahedral sites and prevented interslab spacing expansion by screening the electrostatic repulsion. The same contraction was observed in NaFeO_2 -based materials when a large number of Na-ions are removed, and the $\text{Fe}^{3+/4+}$ migrate into the tetrahedral and octahedral sites in the Na layer.^[24] The case of NaLRNMC4.6 suggests that the migration happens at the beginning of de-sodiation with large amount of Na still remaining in the Na layer, implying that the migration happens more easily than the case of NaFeO_2 , most probably due to the oxygen and TM vacancies in NaLRNMC4.6.

Simulation results (see below) show that 1) the structure that leads to the dampening of the peak during the in situ measurement process is likely metastable, which tends to relax during the ex situ XRD measurement; 2) the loss of order mainly happens along the c-axis, which could be a result of TM layer distortion or TM migrations that disturb the local ordering.^[25] The inhibition of the O3 to P3 phase transition of NaLRNMC is consistent with the solid-solution charge/discharge behavior observed in Figures 1. The good performance at high rate (Supporting Information, Figure S3c–f, 130 mAh g^{-1} capacity with 65 % retention after 1000 cycles at 250 mA g^{-1}) also corroborates that the presence of oxygen vacancies and metal oxide layer distortions lower the Na-ion diffusion barrier.^[26] Galvanostatic intermittent titration (GITT) result shows that the Na-ion diffusion rate is in the magnitude of $10^{-11} \text{ cm}^2 \text{ s}^{-1}$ over the majority of the charging process (Supporting Information, Figure S9). It drops to about $6 \times 10^{-12} \text{ cm}^2 \text{ s}^{-1}$ at the end of charge when the interlayer spacing drops to ca. 5.0 Å. Yet, it is still higher than many of the reported values.^[27] The peak shifts back to lower angle during 2nd sodiation, demonstrating good reversibility of this process.

Magic-angle-spinning nuclear magnetic resonance (MAS-NMR) and X-ray absorption (XAS) have been used to understand the local environment of the remaining Li and the TM migration process. Figure 2 a shows the ⁷Li MAS-NMR results of pristine LRNMC and fully sodiated NaLRNMC4.6. In the pristine LRNMC, two sets of resonances are observed centered around 1500 ppm and 750 ppm, respectively. The peaks at 750 ppm are assigned to the Li in the Li layers, and

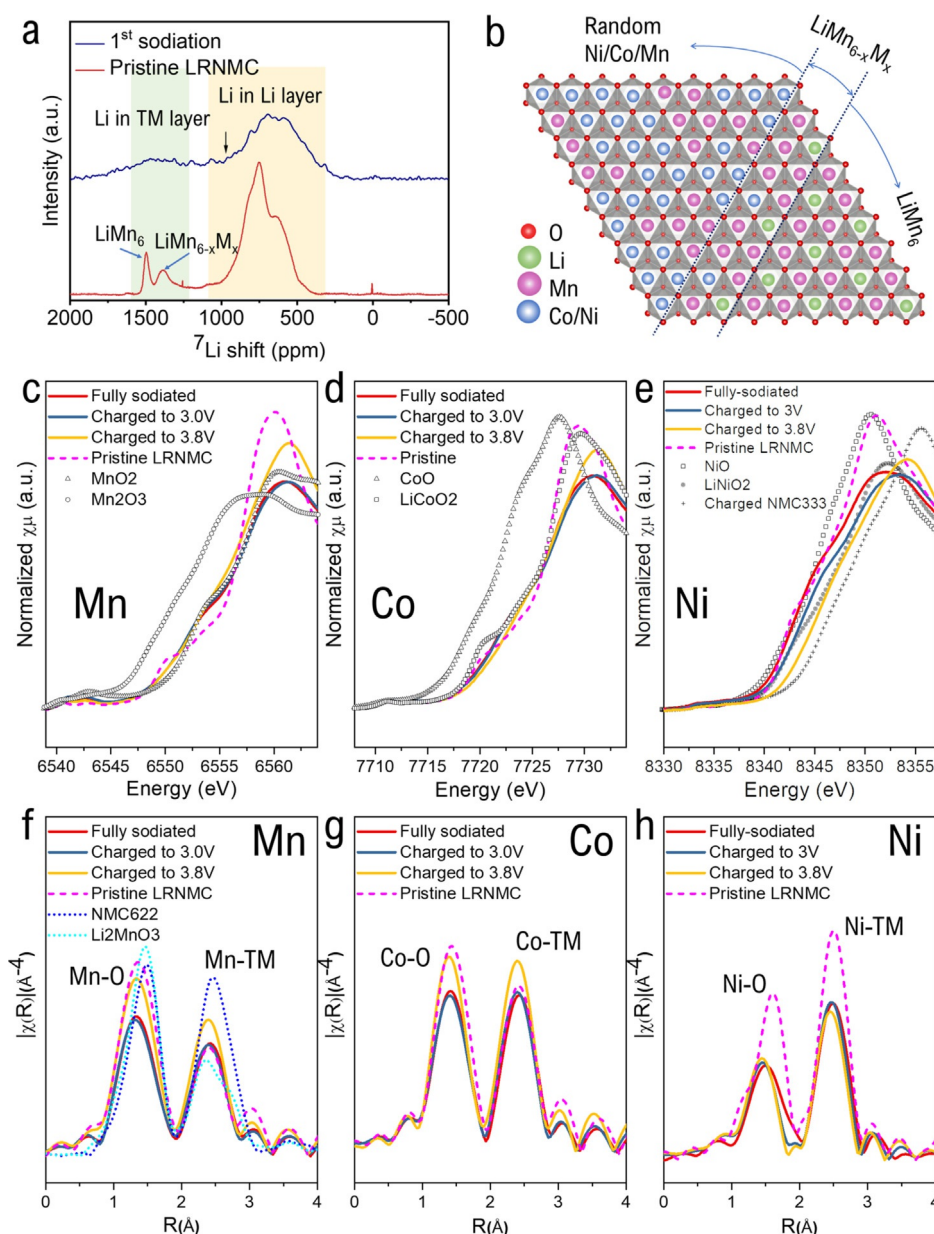


Figure 2. a) ^7Li MAS-NMR results of pristine LRNMC and NaLRNMC at first sodiation state. b) Illustration of the domains with random TM distribution and LiMn_6 ordering in the TM layer of LRNMC. c)–e) XANES data of Mn, Co and Ni K-edges for the ex situ sample. Spectra of reference oxides with known TM valences are also shown for comparison. f)–h) ft-EXAFS data of ex situ samples. Mn ft-EXAFS data includes references ($\text{LiNi}_{0.6}\text{Mn}_{0.2}\text{Co}_{0.2}\text{O}_2$ and Li_2MnO_3) data. In $\text{LiNi}_{0.6}\text{Mn}_{0.2}\text{Co}_{0.2}\text{O}_2$ (NMC622), the coordination number of Mn-TM is 6 and in Li_2MnO_3 it is around 3.

the ones at about 1500 ppm are assigned to the Li in the TM layer. The peak at 1500 ppm originates from LiMn_6 ordering, and the one at 1350 ppm is from $\text{LiMn}_{6-x}\text{M}_x$, with M being either Ni or Co, as illustrated in Figure 2b.^[28] In NaLRNMC4.6 at the 1st sodiation state, the two sets of peaks are still observable, with low sensitivity owing to significantly reduced amount of Li. Considering the actual de-lithiation capacity has exceeded the theoretical de-lithiation capacity as calculated in the Supporting Information, Figure S2, these remaining Li are possibly the ones migrated into the tetrahedral sites in the Li layer during de-lithiation. They are removed out of the original position but stayed in the

material. Upon sodiation, they could either return to the TM layer or continue to migrate into the next octahedral site in the Li layer. The resonance corresponding to Li in the Li layer becomes broader due to more disordered environment with the introduction of Na. The resonances related to the Li in TM layer are also dampened and broadened because of the random distribution of Li, the LiMn_6 feature resonance has largely disappeared, corroborating the disruption of LiMn_6 ordering upon sodiation, likely due to the distortion of the TMO_2 layer as seen from the in situ XRD results. Furthermore, no apparent evidence has shown that there is tetrahedrally coordinated Li, which is supposed to locate at ca.

930 ppm marked by the arrow.^[28] After the de-lithiation of pristine LRNMC, the Li removed from the TM layer can partially return to the TM layer upon lithiation, the LiMn₆ ordering can persist for a couple of cycles, after which the Li and TM become disordered.^[15a,29] However, the case becomes very different when Na intercalates. The large size of Na makes it hardly possible to migrate into the TM layer vacancies, thus the Li (or TM if considering the whole TM layer) vacancies left in the TM layers become disordered in the initial full sodiation.

X-ray absorption near edge structure (XANES) can clearly reveal the TM cation valence and is commonly used to study charge compensation mechanism for battery materials.^[15b] Ex situ Mn, Co and Ni K-edge XANES of NaLRNMC at fully sodiated, charged to 3 V and charged to 3.8 V states, along with some standard metal oxides are shown in Figure 2c–e. The Mn K edge XANES in Figure 2c reveals that Mn does not show obvious valence change upon charging, it stays at 4+ all the time. Co K edge XANES in Figure 2d shows that minor oxidation has taken place when charged to 3.8 V. The Ni K edge XANES, however, displays very drastic change, as shown in Figure 2e. The fully sodiated NaLRNMC has very close Ni valence with that of pristine LRNMC, which is between 2+ and 3+. When charged to 3.0 V, the valence becomes close to that of LiNiO₂ with 3+ valence state. Further charging to 3.8 V shows continuous shift to higher energy position located between LiNiO₂ (3+) and charged LiNi_{1/3}Co_{1/3}Mn_{1/3}O₂ (4+). The XANES results demonstrate that Ni is the major element that contributes to the capacity within the range of 2–3.8 V. The Fourier-transformed (ft) Mn, Co, and Ni K-edge extended X-ray absorption fine structure (EXAFS) of the ex situ samples are presented in Figure 2f–h, Supporting Information, Figures S10, S11 and Tables S3–S5. The nearest metal-oxygen coordination and the second-nearest metal-metal coordination shells are observed in all of them. Figure 2f shows the Mn K edge ft-EXAFS. In a layered cathode material, such as LiNi_{0.6}Mn_{0.2}Co_{0.2}O₂ (NMC622), the first shell coordination number (CN) of Mn is 6, and the second shell CN is also 6. However, in Li₂MnO₃ with Li in the Mn layer, 1/3 of the Mn sites are taken by Li, due to the light scattering of Li to X-ray, the amplitude of the second coordination shell significantly drops, and the CN would be close to 3. This explains why the intensity of the second coordination shell of LRNMC is between that of NMC622 and Li₂MnO₃.^[30] In the fully sodiated NaLRNMC4.6 sample, the first coordination shells of all the three TMs display reduced amplitude, indicating the presence of oxygen vacancies around them. As aforementioned, removing Na out of the structure triggers the TM migration because empty spaces are created in the Na layer. At fully charged state, the TMs that can migrate have migrated. When these TMs return to the TM layer during relaxation, they do not necessarily move to the same site where it was originally removed from. Its second coordination shell CN should increase because of the redistribution of TM vacancies. Of the three TMs at charged states, both Mn and Co show an increase of amplitude in their second coordination shell peak that are even higher than the pristine LRNMC, whereas Ni does not show such feature. The results indicate that Mn and

Co are more favorable to migrate than Ni in the process. This is within expectation since Ni at higher oxidation state is known to be unfavorable to squeeze into the tetrahedral site in layered metal oxides.^[31] The limited change of the TM-O and TM-TM coordination upon half desodiation can be ascribed to 1) the instability of TMs on the tetrahedral sites in layered sodium materials and relax to its original layer, despite not necessarily to the same site;^[19b] 2) the amount of migrated TMs falls below the detection limit of XANES/EXAFS while its change is significant enough to stabilize the O3 structure.

To the best of our knowledge, except this current compound, O3-NaTiO₂^[32] and O3-NaMnO₂,^[23] all other cyclable O3-NaTMO₂ (without TM vacancy) become P3 or P'3 (P3 with monoclinic distortion) at Na_{1/2}TMO₂.^[24,33] To understand how the O3-P3 biphasic reaction is circumvented in the de-sodiation process of NaLRNMC, theoretical simulation study was carried out. Combined with other experimental evidences discussed above, we therefore choose Na_{1/2}Mn_{9/16}Ni_{1/8}Co_{1/8}□_{3/16}O₂ with TM migrations as the model system to study the energy preference on O3 and P3 phases.

In a typical initial structure before DFT relaxations as shown in Figure 3a, the structure exhibits either O3 or P3 stacking with 2 TMs close to the TM vacancies migrated to the sodium layer. The example structure in Figure 3a was fully relaxed to the structure in Figure 3b, whose sodium sites are largely distorted. In Figure 3c, we summarize the sodium environments and structure details in the relaxed structures. Traditional prismatic, octahedral, and tetrahedral sites are found, but a large portion of the sodium environments are distorted, whose number of Na–O bonds can deviate from 6. In some rare cases, Na ions can also squeeze into the TM layer, possibly due to the large amount of TM vacancies. Prismatic site and octahedral site Na ions can sometimes be close to each other without a distorted site sodium in between, which can strain the layered structure locally and increase the energy. We define such an empty space in between as the P-O interface. Figure 3c also shows DFT energies over a metric related to the distribution of the 8 sodium environments. The more concentrated to certain type of Na environment the structure is, the larger the value of the metric. The largest end of the metric corresponds to major O3 phase (two 7O1P and one 7O1d) or major P3 phase (7P1TM), while the smallest end corresponds to a phase with 4 mixed types of Na environments (2O2P3D1T). Other structures are distributed in between. Major P3 phase (7P1TM) has the lowest energy, suggesting that major O3 phase and other phases with mixed O sites are metastable at Na composition of 1/2. The energy range of these structures is as large as 215 meV/TMO₂. The blue arrow is a guide of eye along which the number of octahedral sites decreases, while that of prismatic sites increases, which can be understood as the evolution pathway from O3 to P3 phase through a series of metastable phases with distorted sites.

We further use linear regression to express the DFT energy as the following Equation (1):

$$\text{DFT energy} = \sum_{\text{site type}} \text{site energy} \times \text{site quantity} \quad (1)$$

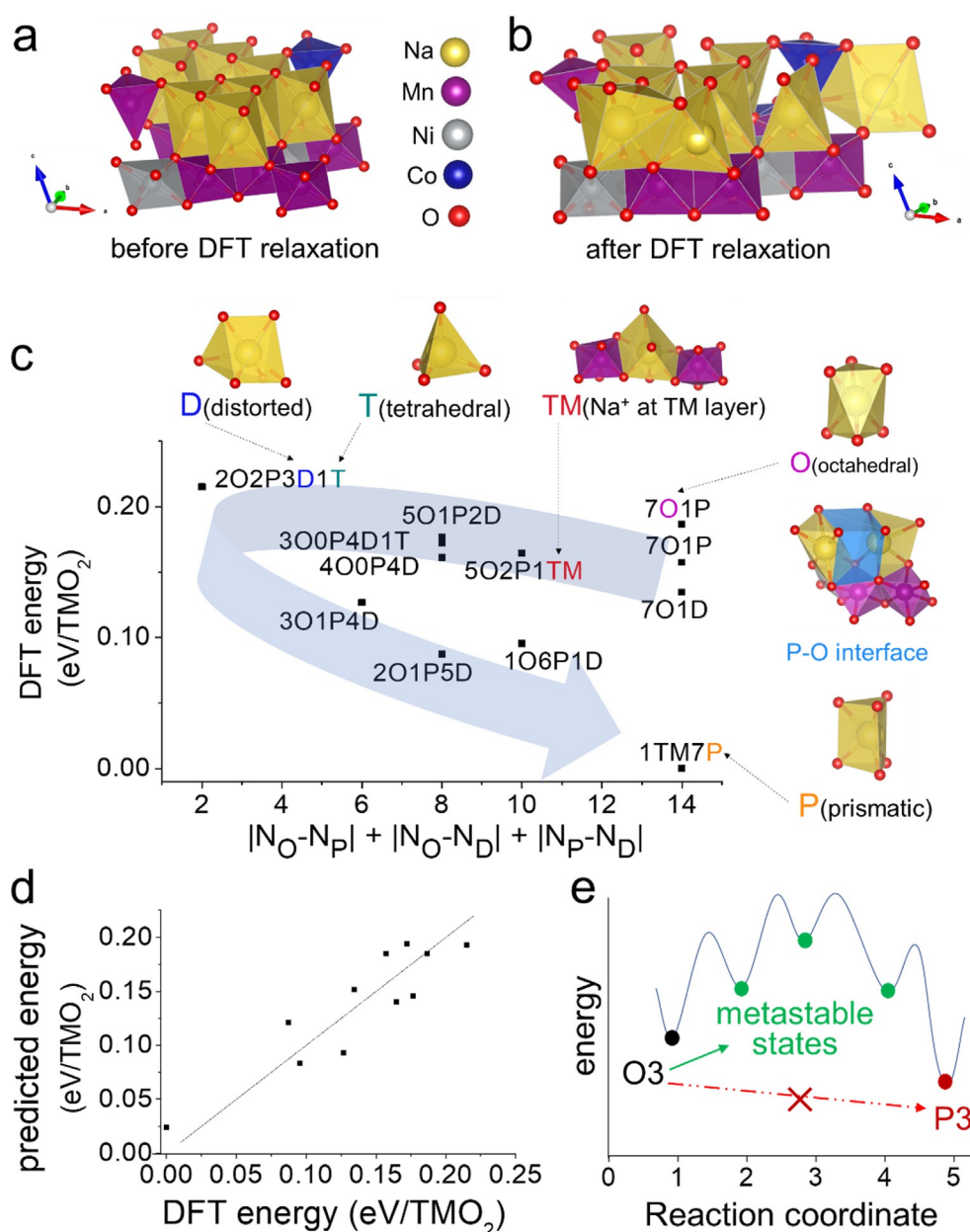


Figure 3. DFT simulations on $\text{Na}_{1/2}\text{Mn}_{9/16}\text{Ni}_{1/8}\text{Co}_{1/8}\square_{3/16}\text{O}_2$ with transition metal migrations. a) An example structure before DFT relaxation, and b) the structure after DFT relaxation. c) DFT energy versus a metric describing the distribution of the 8 sodium occupied sites among different local environments. The metric for each data point is calculated by counting the sodium environments. The blue curved arrow is a guide of eye to illustrate the possible evolution pathway starting from O3 through a series of distorted metastable states with reducing O and increasing P sites. Representative sodium environments are shown aside: P for prismatic site, O for octahedral site, T for tetrahedral site, D for distorted site, and TM for sodium at TM layer (rare case). The empty site between two close P and O site sodium ions without a D site sodium is defined as the P-O interface, but not counted explicitly. d) Predicted energies based on linear regression using Equation (2) versus DFT energies. e) Illustration of the mechanism about how the O3-P3 biphasic reaction is prevented.

The result of the linear regression is shown in Equation (2) and Figure 3d. It shows a good linear fit with Equation (2), which demonstrates that prismatic sites and distorted sites are low in energy (negative coefficients), while octahedral sites and P-O interface are high in energy (positive coefficients).

$$\text{DFT energy} = -0.02 N_P - 0.01 N_D - 0.05 N_{\text{TM}} - 0.001 N_O - 0.01 N_{\text{P-O interface}} + 0.08 N_T + 0.158 \quad (2)$$

Normally the O3-P3 biphasic reaction is initiated by the gliding of TMO₂ layer,^[34] however the migrated TM ions could impede such a global gliding.^[35] Once local P sites with low energies are formed instead, the high energy P-O interface will prefer to transform into distorted sites, forcing the system to evolve through a metastable pathway with

distorted metal oxide layers. Figure 3e illustrates the proposed energy evolution in the O3-P3 biphasic reaction conditioning TM migrations. Such metastable states could trap the structure and prevent the evolution to the global P stacking. In practice, these prismatic and distorted sites could randomly distribute in the main O3 phase at all Na compositions, so that the pure O3 pattern in X-ray diffraction is maintained yet less intense in the in situ XRD measurement. The fact that ex situ XRD shows intense peaks with sharper full width at half maximum (FWHM) corroborates the presence of meta-stable intermediate phases with the in situ migrated TM ions largely relaxing back to the TMO₂ layer in any ex situ measurements.

Long term structural stability and the reversibility of TM migration were evaluated by analyses of the sXRD and X-ray pair distribution function (xPDF) analysis of cycled samples. Figure 4a displays the sXRD pattern of NaLRNMC4.6 at the 101st sodiation states fitted by Le Bail method, the fitting results are shown in the Supporting Information, Table S2. The sample still shows a mixture of two O3 phases, corresponding to the same ones with the 1st sodiation, suggesting that the O3 phase is stable during cycling. X-ray pair distribution function (xPDF) analysis of the pristine LRNMC, NaLRNMC4.6 at 1st and 101st sodiation states was carried out to study the change of local structures with Na intercalation, as shown in Figure 4b. In the pristine LRNMC, the shortest bond located at 1.95 Å represents the Li/TM-O correlations in the LiO₆ and TMO₆ octahedra. The second peak at 2.9 Å corresponds to the Li/TM-Li/TM correlations. At the 1st sodiation state, the intensity of the first peak did not drop much despite the removal of Li due to the light

scattering power of Li. An extra peak emerges at 2.32 Å, it can be assigned to the correlation between Na and O in the NaO₆ octahedra. The third peak has shown a positive shift of 0.1 Å owing to the larger size of Na, which leads to an expansion of the unit cell. The peak at 3.2 Å is the correlation between Na and TMs. The xPDF pattern of the sample at 101st sodiation shows no peak position changes. The only observable difference is that the amplitude of the third peak drops slightly, presumably due to less intercalated Na, which agrees well with the sXRD pattern that there is more O3b' phase in the sample after 101st sodiation compared to the 1st sodiation. The negligible difference further demonstrates that the migration of TMs during the cycling is largely reversible, at least the amount of irreversible migration is beyond the detection limit of synchrotron XRD, PDF and XANES. In the case of NaFeO₂, Fe^{3+/4+} migration to the tetrahedral site was also observed, it was concluded that the Fe acts as a pin to prevent layer gliding. However, that migration is irreversible, and these tetrahedral Fe-ions block the diffusion of Na-ions, leading to a concentration gradient, so the cycling stability is poor despite forbidden phase transition.^[36]

Conclusion

We have carried out a systematic study to validate the possibility of improving the manganese-rich layered Na-ion cathodes by introducing TM and oxygen vacancies. Using the electrochemically de-lithiated LRNMC as the model material, a cathode that can have a sodiation capacity of ca. 220 mAh g⁻¹ was demonstrated. It can deliver ca. 160 mAh g⁻¹ specific capacity between 2–3.8 V with > 86% retention over 250 cycles. The combined experimental and computational study show that the migration activated by TM and oxygen vacancies has led to multiple anomalous phenomena that are related to the design of high-performance layered cathode materials. First, the migration of TM happens right after desodiation, owing to the rich TM and oxygen vacancies that can reduce the energy barrier. This observation is different from the case of NaFeO₂, in which the migration only occurs when relatively large amount of Na is removed, and the process is largely irreversible. Second, the presence of TMs in the tetrahedral sites in the Na layer leads to a contraction of the interlayer spacing upon de-sodiation, which is against conventional materials that experience an expansion instead, but the diffusion of Na-ions was not impacted. This fast Na-ion diffusion can be attributed to the presence of oxygen vacancies and metal oxide layer distortions of the metastable phases in the structure that significantly reduce the energy required for Na-ions to migrate. Third, the formation of multiple intermediate metastable phases that have both O and P-type Na occupancies in the same layer has a broad energy distribution, thus increasing the kinetic barrier of the O3-P3 phase transition. This argument has been experimentally supported by the different (003) peak intensities in the ex situ and in situ XRD patterns. Ex situ XRD measures relaxed structures, thus the (003) peak is very sharp and intense. However, in situ XRD measures a dynamic process where the metastable phases are present, thus the (003) peak

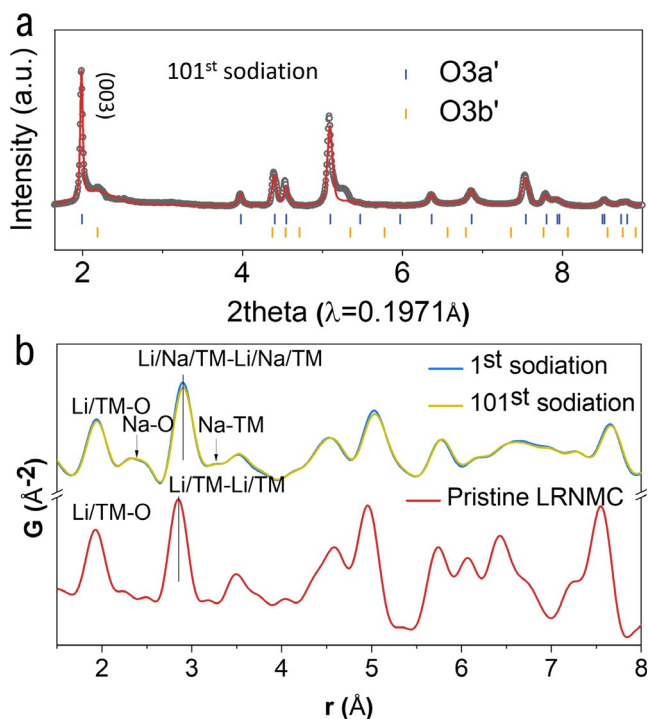


Figure 4. a) Le Bail fitting of the 101st sodiation sample using two O3 phases termed as O3a' and O3b'. b) X-ray PDF of pristine LRNMC, NaLRNMC at 1st and 101st sodiation states.

is very broad. Our picture differs from the reasons for the delayed O-P phase transition in NaFeO_2 and the P-O phase transition in Li-doped $\text{Na}_x[\text{Li}_y\text{Ni}_z\text{Mn}_{1-y-z}]\text{O}_2$, which was argued to be the pinning effect of the Fe in the tetrahedral sites or the Li in the octahedral sites.^[36,37] Despite the electrochemical Li/Na exchange approach in this study is not suitable for scaling up, future work using a chemical ion-exchange/oxidation approach or precise vacancy control is open for exploration.^[38] It is thus foreseen that introducing TM and oxygen vacancies during the material synthesis with careful composition and phase control would be an inspiring approach to develop high-performance layered sodium cathode materials.

Acknowledgements

X.L.L. would like to thank the support from the U.S. Department of Energy (DOE) Office of Electricity (Contract No. 70247A). Pacific Northwest National Laboratory is a multiprogram laboratory operated by Battelle Memorial Institute for the DOE under Contract DE-AC05-76RL01830. S.T., X.-Q.Y., and E.H. at Brookhaven National Laboratory are supported by Assistant Secretary for Energy Efficiency and Renewable Energy, Vehicle Technology Office of the U.S. DOE, through the Advanced Battery Materials Research (BMR) Program, including Battery500 Consortium under contract DE-SC0012704. Y.W. and Xin Li are supported by Data Science Initiative Competitive Research Fund at Harvard (HDSI). F.L. and Y.Z. acknowledge the National Science Foundation for supporting the work at Virginia Tech (No. CBET-1912885). This research used beamline 7-BM (QAS) and 28-ID-2 (XPD) of the National Synchrotron Light Source II, U.S. DOE Office of Science User Facilities operated for the DOE Office of Science by Brookhaven National Laboratory under Contract No. DE-SC0012704. Research at the Argonne National Laboratory was funded by the US Department of Energy (DOE), Vehicle Technologies Office. Support from T. Duong of the US DOE's Office of Vehicle Technologies Program is gratefully acknowledged. Use of the Advanced Photon Source, an Office of Science User Facility operated for the DOE Office of Science by Argonne National Laboratory, was supported by DOE under contract no. DE-AC02-06CH11357. All solid-state NMR experiments were performed at the National High Magnetic Field Laboratory. The National High Magnetic Field Laboratory is supported by National Science Foundation through NSF/DMR-1644779 and the State of Florida. Computations were supported by the Extreme Science and Engineering Discovery Environment (XSEDE) and the Odyssey cluster of the FAS Division of Science Research Computing Group at Harvard University.

Conflict of interest

The authors declare no conflict of interest.

Keywords: layered materials · metastability · phase transitions · sodium-ion batteries · vacancies

- [1] a) D. Saurel, B. Orayech, B. Xiao, D. Carriazo, X. Li, T. Rojo, *Adv. Energy Mater.* **2018**, *8*, 1703268; b) Y. You, A. Manthiram, *Adv. Energy Mater.* **2018**, *8*, 1701785; c) G.-L. Xu, R. Amine, A. Abouimrane, H. Che, M. Dahbi, Z.-F. Ma, I. Saadoune, J. Alami, W. L. Mattis, F. Pan, Z. Chen, K. Amine, *Adv. Energy Mater.* **2018**, *8*, 1702403; d) B. Xiao, T. Rojo, X. Li, *ChemSusChem* **2019**, *12*, 133–144; e) H. S. Hirsh, Y. Li, D. H. S. Tan, M. Zhang, E. Zhao, Y. S. Meng, *Adv. Energy Mater.* **2020**, *10*, 2001274.
- [2] N. Palaniyandy, *Curr. Opin. Electrochem.* **2020**, *21*, 319–326.
- [3] a) C. Delmas, D. Carlier, M. Guignard, *Adv. Energy Mater.* **2021**, *11*, 2001201; b) R.-M. Gao, Z.-J. Zheng, P.-F. Wang, C.-Y. Wang, H. Ye, F.-F. Cao, *Energy Storage Mater.* **2020**, *30*, 9–26.
- [4] M. Guignard, C. Didier, J. Darriet, P. Bordet, E. Elkaim, C. Delmas, *Nat. Mater.* **2013**, *12*, 74–80.
- [5] N. Yabuuchi, M. Kajiyama, J. Iwatate, H. Nishikawa, S. Hitomi, R. Okuyama, R. Usui, Y. Yamada, S. Komaba, *Nat. Mater.* **2012**, *11*, 512–517.
- [6] J. Song, K. Wang, J. Zheng, M. H. Engelhard, B. Xiao, E. Hu, Z. Zhu, C. Wang, M. Sui, Y. Lin, D. Reed, V. L. Sprenkle, P. Yan, X. Li, *ACS Energy Lett.* **2020**, *5*, 1718–1725.
- [7] K. Kubota, S. Kumakura, Y. Yoda, K. Kuroki, S. Komaba, *Adv. Energy Mater.* **2018**, *8*, 1703415.
- [8] N. Yabuuchi, K. Kubota, M. Dahbi, S. Komaba, *Chem. Rev.* **2014**, *114*, 11636–11682.
- [9] a) Y. Sun, S. Guo, H. Zhou, *Energy Environ. Sci.* **2019**, *12*, 825–840; b) T. Y. Yu, H. H. Ryu, G. Han, Y. K. Sun, *Adv. Energy Mater.* **2020**, *10*, 2001609; c) P.-F. Wang, Y. You, Y.-X. Yin, Y.-G. Guo, *Adv. Energy Mater.* **2018**, *8*, 1701912.
- [10] a) Y. Xiao, N. M. Abbasi, Y. F. Zhu, S. Li, S. J. Tan, W. Ling, L. Peng, T. Yang, L. Wang, X. D. Guo, Y. X. Yin, H. Zhang, Y. G. Guo, *Adv. Funct. Mater.* **2020**, *30*, 2001334; b) X. Cao, H. Li, Y. Qiao, M. Jia, X. Li, J. Cabana, H. Zhou, *Adv. Mater.* **2020**, *32*, 2004280; c) G. Liang, Z. Wu, C. Didier, W. Zhang, J. Cuan, B. Li, K. Y. Ko, P. Y. Hung, C. Z. Lu, Y. Chen, G. Leniec, S. M. Kaczmarek, B. Johannessen, L. Thomsen, V. K. Peterson, W. K. Pang, Z. Guo, *Angew. Chem. Int. Ed.* **2020**, *59*, 10594–10602; *Angew. Chem.* **2020**, *132*, 10681–10689; d) H. Y. Asl, A. Manthiram, *Science* **2020**, *369*, 140–141.
- [11] a) P. F. Wang, H. R. Yao, X. Y. Liu, J. N. Zhang, L. Gu, X. Q. Yu, Y. X. Yin, Y. G. Guo, *Adv. Mater.* **2017**, *29*, 1700210; b) P. F. Wang, Y. You, Y. X. Yin, Y. S. Wang, L. J. Wan, L. Gu, Y. G. Guo, *Angew. Chem. Int. Ed.* **2016**, *55*, 7445–7449; *Angew. Chem.* **2016**, *128*, 7571–7575.
- [12] a) S. Guo, P. Liu, H. Yu, Y. Zhu, M. Chen, M. Ishida, H. Zhou, *Angew. Chem. Int. Ed.* **2015**, *54*, 5894–5899; *Angew. Chem.* **2015**, *127*, 5992–5997; b) Q. Huang, J. Liu, S. Xu, P. Wang, D. G. Ivey, B. Huang, W. Wei, *Chem. Mater.* **2018**, *30*, 4728–4737.
- [13] R. J. Clément, P. G. Bruce, C. P. Grey, *J. Electrochem. Soc.* **2015**, *162*, A2589–A2604.
- [14] a) E. Hu, X. Yu, R. Lin, X. Bi, J. Lu, S. Bak, K.-W. Nam, H. L. Xin, C. Jaye, D. A. Fischer, K. Amine, X.-Q. Yang, *Nat. Energy* **2018**, *3*, 690–698; b) E. Hu, Y. Lyu, H. L. Xin, J. Liu, L. Han, S. M. Bak, J. Bai, X. Yu, H. Li, X. Q. Yang, *Nano Lett.* **2016**, *16*, 5999–6007.
- [15] a) C. P. Grey, W.-S. Yoon, J. Reed, G. Ceder, *ECS Solid State Lett.* **2004**, *7*, A290; b) B. Xiao, H. Liu, N. Chen, M. N. Banis, H. Yu, J. Liang, Q. Sun, T. K. Sham, R. Li, M. Cai, G. A. Botton, X. Sun, *Angew. Chem. Int. Ed.* **2020**, *59*, 14313–14320; *Angew. Chem.* **2020**, *132*, 14419–14426.
- [16] B. Xiao, B. Wang, J. Liu, K. Kaliyappan, Q. Sun, Y. Liu, G. Dadheech, M. P. Balogh, L. Yang, T.-K. Sham, R. Li, M. Cai, X. Sun, *Nano Energy* **2017**, *34*, 120–130.

- [17] a) E. McCalla, A. W. Rowe, J. Camardese, J. R. Dahn, *Chem. Mater.* **2013**, *25*, 2716–2721; b) R. Shunmugasundaram, R. Senthil Arumugam, J. R. Dahn, *Chem. Mater.* **2015**, *27*, 757–767.
- [18] B. Mortemard de Boisse, S.-i. Nishimura, E. Watanabe, L. Landier, A. Tsuchimoto, J. Kikkawa, E. Kobayashi, D. Asakura, M. Okubo, A. Yamada, *Adv. Energy Mater.* **2018**, *8*, 1800409.
- [19] a) J. Billaud, R. J. Clement, A. R. Armstrong, J. Canales-Vazquez, P. Rozier, C. P. Grey, P. G. Bruce, *J. Am. Chem. Soc.* **2014**, *136*, 17243–17248; b) X. Ma, H. Chen, G. Ceder, *J. Electrochem. Soc.* **2011**, *158*, A1307.
- [20] A. Le Bail, H. Duroy, J. L. Fourquet, *Mater. Res. Bull.* **1988**, *23*, 447–452.
- [21] Y. Xie, H. Wang, G. Xu, J. Wang, H. Sheng, Z. Chen, Y. Ren, C.-J. Sun, J. Wen, J. Wang, D. J. Miller, J. Lu, K. Amine, Z.-F. Ma, *Adv. Energy Mater.* **2016**, *6*, 1601306.
- [22] G.-L. Xu, R. Amine, Y.-F. Xu, J. Liu, J. Gim, T. Ma, Y. Ren, C.-J. Sun, Y. Liu, X. Zhang, S. M. Heald, A. Solhy, I. Saadoune, W. L. Mattis, S.-G. Sun, Z. Chen, K. Amine, *Energy Environ. Sci.* **2017**, *10*, 1677–1693.
- [23] X. Chen, Y. Wang, K. Wiaderek, X. Sang, O. Borkiewicz, K. Chapman, J. LeBeau, J. Lynn, X. Li, *Adv. Funct. Mater.* **2018**, *28*, 1805105.
- [24] X. Li, Y. Wang, D. Wu, L. Liu, S.-H. Bo, G. Ceder, *Chem. Mater.* **2016**, *28*, 6575–6583.
- [25] B. Silván, E. Gonzalo, L. Djuandhi, N. Sharma, F. Fauth, D. Saurel, *J. Mater. Chem. A* **2018**, *6*, 15132–15146.
- [26] a) D. Qian, B. Xu, M. Chi, Y. S. Meng, *Phys. Chem. Chem. Phys.* **2014**, *16*, 14665–14668; b) X. Chen, S. Hwang, R. Chisnell, Y. Wang, F. Wu, S. Kim, J. W. Lynn, D. Su, X. Li, *Adv. Funct. Mater.* **2018**, *28*, 1803896.
- [27] N. A. Katcho, J. Carrasco, D. Saurel, E. Gonzalo, M. Han, F. Aguesse, T. Rojo, *Adv. Energy Mater.* **2017**, *7*, 1601477.
- [28] M. Jiang, B. Key, Y. S. Meng, C. P. Grey, *Chem. Mater.* **2009**, *21*, 2733–2745.
- [29] R. Wang, X. He, L. He, F. Wang, R. Xiao, L. Gu, H. Li, L. Chen, *Adv. Energy Mater.* **2013**, *3*, 1358–1367.
- [30] M. M. Thackeray, S.-H. Kang, C. S. Johnson, J. T. Vaughey, R. Benedek, S. A. Hackney, *J. Mater. Chem.* **2007**, *17*, 3112–3125.
- [31] a) B. Xiao, H. Liu, J. Liu, Q. Sun, B. Wang, K. Kaliyappan, Y. Zhao, M. N. Banis, Y. Liu, R. Li, T. K. Sham, G. A. Botton, M. Cai, X. Sun, *Adv. Mater.* **2017**, *29*, 1703764; b) N. Twu, M. Metzger, M. Balasubramanian, C. Marino, X. Li, H. L. Chen, H. Gasteiger, G. Ceder, *Chem. Mater.* **2017**, *29*, 2584–2593.
- [32] D. Wu, X. Li, B. Xu, N. Twu, L. Liu, G. Ceder, *Energy Environ. Sci.* **2015**, *8*, 195–202.
- [33] a) S.-H. Bo, X. Li, A. J. Toumar, G. Ceder, *Chem. Mater.* **2016**, *28*, 1419–1429; b) J. C. Kim, D. H. Kwon, J. H. Yang, H. Kim, S. H. Bo, L. Wu, H. Kim, D. H. Seo, T. Shi, J. Wang, *Adv. Energy Mater.* **2020**, *10*, 2001151.
- [34] J. L. Kaufman, J. Vinckeiviūtė, S. Krishna Kolli, J. Gabriel Goiri, A. Van der Ven, *Philos. Trans. R. Soc. London Ser. A* **2019**, *377*, 20190020.
- [35] B. Song, E. Hu, J. Liu, Y. Zhang, X.-Q. Yang, J. Nanda, A. Huq, K. Page, *J. Mater. Chem. A* **2019**, *7*, 1491–1498.
- [36] E. Lee, D. E. Brown, E. E. Alp, Y. Ren, J. Lu, J.-J. Woo, C. S. Johnson, *Chem. Mater.* **2015**, *27*, 6755–6764.
- [37] J. Xu, D. H. Lee, R. J. Clément, X. Yu, M. Leskes, A. J. Pell, G. Pintacuda, X.-Q. Yang, C. P. Grey, Y. S. Meng, *Chem. Mater.* **2014**, *26*, 1260–1269.
- [38] a) K. Kang, Y. S. Meng, J. Breger, C. P. Grey, G. Ceder, *Science* **2006**, *311*, 977–980; b) D. Eum, B. Kim, S. J. Kim, H. Park, J. Wu, S. P. Cho, G. Yoon, M. H. Lee, S. K. Jung, W. Yang, W. M. Seong, K. Ku, O. Tamwattana, S. K. Park, I. Hwang, K. Kang, *Nat. Mater.* **2020**, *19*, 419–427.

Manuscript received: December 11, 2020

Revised manuscript received: January 10, 2021

Accepted manuscript online: January 21, 2021

Version of record online: March 1, 2021